SUNFLOWER PLANTING MACHINERY ELECTRIFICATION TRANSFORMATION AND CONTROL SYSTEM DESIGN

/

葵花种植机械电动化改造及控制系统设计

Guoxing CAI[1)], Haijun LI[*1)], Dabo LU[2)], Renjie WANG[1)], Kaiyuan WANG[1)], Subo QIN[1)], Zhiqiang WU[1)]

[1)] College of Electrical and Mechanical Engineering, Inner Mongolia Agricultural University, Hohhot / China;

[2)] Inner Mongolia Dabo Jintian Machinery Company Limited, Bayannur / China

Tel: +86 13848129323; E-mail: lhj70927@sina.com

Corresponding author: Haijun Li

DOI: https://doi.org/10.35633/inmateh-72-06

Keywords: *sunflower mulching planter, kinematic modeling, control system, Linux system*

ABSTRACT

This research aimed to address the issue of physical damage caused by long-term work in high-saline fields by electrifying sunflower growing machinery and designing control systems. Firstly, the method of establishing the equation of motion is used to obtain the parameters to carry out motorization modification, and then the control system is built using STM32 as the main controller, which has the functions of control, data acquisition, and alarm. The feasibility and stability of the study are verified by using a model vehicle to conduct tests of straight-line driving and steering in a simulated high-saline field.

摘要

本研究的重点是通过对葵花种植机械进行电气化改造和设计控制系统解决工作人员长时间在高盐碱地工作对身体有损伤的问题。首先采用建立运动方程的方法获取参数从而进行电动化改造，然后使用 STM32 作为主控制器搭建控制系统，该系统具有控制、数据采集和报警的功能。使用模型车在模拟的高盐碱地进行直线行驶和转向的试验验证该研究的可行性和稳定性。

INTRODUCTION

Seeders are widely used in agriculture, especially in harsh environments to reduce the labor intensity of manual seeding to a large extent. With the development of the agricultural economy, automatic control technology, and intelligent technology in agricultural production in a wide range of applications, the economy and precision of the seeding machine have reached a higher level *(Yang et al., 2022; Bi Yajuan, 2021; Liang et al., 2024; Chen et al., 2024)*. Sunflowers can grow in slightly acidic and alkaline environments with a pH of 6.0 to 7.5, making them well-suited to growing in saline soils. However, they still need to be watered heavily in the spring before planting to reduce salinity *(Fatima et al., 2021)*. There are many problems such as traveling difficulty, insufficient steering ability, poor steering accuracy, serious skidding, and so on, which cause a high degree of dependence on manual labor when the planter works in the saline land after the watering to reduce the salinity.

In agricultural machinery, Internal Combustion Engine (ICE) is usually fueled with diesel, although some bio-fuel blends have been proposed in the literature to reduce emissions *(Lovarelli et al., 2019)*. Some scholars proposed that the electric drive intelligent high-speed precision sowing machine still needs a tractor for traction *(Liang et al., 2023)*. Some scholars have investigated fully electric small-family agricultural tractors using a single permanent magnet motor and lead-acid batteries, which can permit changes in track width and ground clearance *(Das et al., 2019; Gurusamy et al., 2015; Brenna et al., 2018)*. This paper takes the 2BQKS-2 diesel self-propelled air-absorbing sunflower mulching seeder produced by Inner Mongolia Dabo Jintian Machinery Co. Ltd. as a prototype for electrification transformation, and the transformed seeder is easier to realize the control of speed and direction. Moreover, the motorized transformation of the seeder lays the foundation for the subsequent intelligent transformation, and the remote control of the seeder by the staff can avoid skin irritation, and respiratory and neurological injuries caused by working on the saline soil for a long time.

Guoxing Cai, M.S. Stud. Eng.; Haijun Li, Prof, M.S. ENG.; Renjie Wang, M.S. Stud. Eng; Kaiyuan Wang, M.S. Stud. Eng; Subo Qin, M.S. Stud. Eng; Zhiqiang Wu, MS. Stud. Eng.; Dabo Lu, P&D*

The control system uses the Proportion-Integration-Differentiation (PID) algorithm, but the steering controller under the PID method has problems of large overshoot and low accuracy *(Xiong et al., 2020; Li et al., 2019; Shen et al., 2019)*. Therefore, the kinematic analysis of slip steering under the world coordinate system is carried out first, and the control parameters of the PID algorithm are optimized according to the equations of motion, to solve the two problems mentioned above, and also to better solve the problems of misalignment of crop rows and inconsistency of row spacing, which facilitates the subsequent mechanization of fertilizer application, drug spreading, harvesting and other mechanized operations.

MATERIALS AND METHODS

Slip steering kinematic analysis

The steering mode of the seeder studied in this paper is selected to increase the steering mode, that is, the speed of the outer wheels is accelerated, and this steering mode can keep the speed of the geometric center of the vehicle unchanged, to be closer to the true steering motion of the vehicle *(Ding Dong, 2021)*. The 2BQKS-2 self-propelled air-absorbent sunflower mulching planter is center-symmetric, as shown in Fig. 1. The body size of the seeder is 2.6X1.3 m, wheelbase is 1.1 m, axle distance is 2 m, the weight of the whole machine is about 460 kg, and the speed is 4-7 km/h. The analysis after that does not take into account the effect of different terrain on the friction of the wheels and the steering radius, and the friction coefficient of the tires and the ground is stable and unchanged, the rotation speeds of the wheels at the same side are the same and the center of gravity of the vehicle does not change with the steering. The traveling path of the planter is shown in Fig. 2.

Fig. 1 - 2BQK-2 type sunflower seeder

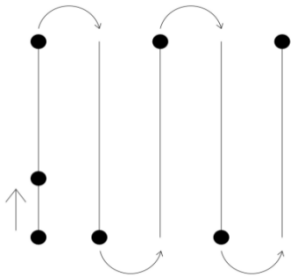

Fig. 2 - Traveling path of the planter

Straight-line travel is achieved when the speed and direction of the vehicle's inner and outer tires are aligned. The speed of the collection center when the vehicle travels in a straight line is also equal to the linear speed of the wheels, and the equation of linear motion is shown in Equation (1):

$$\begin{bmatrix} V_1 \\ V_2 \\ V_3 \\ V_4 \end{bmatrix} = \begin{bmatrix} R_1 \\ R_2 \\ R_3 \\ R_4 \end{bmatrix} \quad (1)$$

where: V_i is the linear velocity of the wheel, [m/s]; R_i is the corresponding angular velocity of the wheel, [rad/s]; 1 is the left front wheel; 2 is the right front wheel; 3 is the left rear wheel; 4 is the right rear wheel.

The slip steering process of a four-wheeled vehicle can be viewed as a combination of lateral and vertical motions, as shown in Fig. 3.

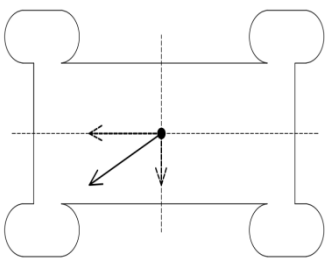

Fig. 3 - Slip steering synthesis

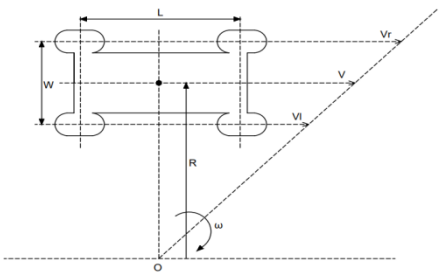

Fig. 4 - Schematic of steering with a large radius

Take left steering as an example, when the inner and outer wheels of the planter rotate at different speeds in the same direction when the movement relationship is shown in Fig. 4.

Taking clockwise steering as the positive direction and O as the center of rotation, then theoretically the speed of the geometric center of the planter, the angular speed of rotation, and the radius of steering are calculated as follows:

$$V = \frac{V_r + V_l}{2} \tag{2}$$

$$\omega = \frac{V}{R} = \frac{V_l}{R - \frac{\omega}{2}} = \frac{V_r}{R + \frac{\omega}{2}} \tag{3}$$

$$R = \frac{W}{2} \cdot \frac{V_r + V_l}{V_r - V_l} > \frac{W}{2} \tag{4}$$

where:

V is the speed of the geometric center, [m/s]; ω is rotational angular velocity, [rad/s]; R is turning radius, [m]; W is the wheelbase, [m]; L is the axle distance, [m]; V_l is the speed of the left wheel, [m/s]; V_r is the speed of the right wheel, [m/s].

When the inner and outer wheels of the planter rotate at different speeds in different directions and also in different simultaneous motion relationships as shown in Figure 5, the theoretical speed of the geometric center of the vehicle and the angular velocity of rotation are shown in Equations 2 and 3 with the direction of the right-hand wheel as the positive direction. The theoretical steering radius of the whole vehicle is:

$$R = \frac{W}{2} \bullet \frac{V_r + V_l}{V_r - V_l} < \frac{W}{2} \tag{5}$$

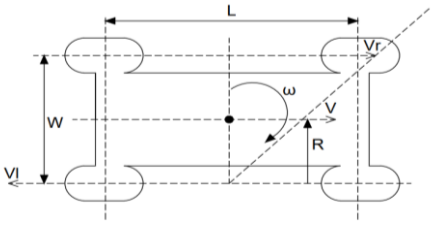

Fig. 5 - Schematic of steering with a small radius

When the inner and outer wheels of the planter rotate at the same speed in different directions, the body speed V=0 from Equation 2, that is, in-situ steering, in the ideal case the steering radius R=0, and the formula for angular velocity is as follows:

$$\omega = \frac{V_r}{\frac{W}{2}} = -\frac{V_l}{\frac{W}{2}} \tag{6}$$

Slip Steering Dynamics Analysis

The actual working environment is more complex, and the analysis of the drive of the planter in different situations allows for better motorization and is also the basis of the control system. The following analysis is carried out under ideal conditions.

When the vehicle is traveling in a straight line, it must be ensured that the total driving force of the driving wheels is greater than the friction force between the wheels and the ground. From the perspective of dynamics analysis, when steering the two sides of the wheels will produce a driving force difference, the formation of steering driving moment, the direction of the moment points to the inside of the wheel. At the same time, a steering resistance moment is generated between the tire and the ground, whose direction is opposite to the driving moment. To realize steering, the driving moment must be greater than the resistance moment.

The rolling resistance coefficient is assumed to be constant when steering, the same as when traveling in a straight line. Rolling resistance is always opposite to the direction of wheel rotation, and the kinematic characteristics of the vehicle are different depending on the steering radius. When steering, the moment generated by rolling resistance may be the driving moment or resistance moment. When steering with a large radius, the direction of rotation of the tires on both sides and the direction of the moment generated by rolling resistance are the same; while when steering with a small radius, the direction of rotation of the tires on both sides is different and the direction of the moment generated by rolling resistance is opposite.

When a planter is steered, the tires create a sliding motion in the soil and therefore are also affected by sliding resistance. So, the seeder is affected by rolling resistance and sliding resistance when steering in a large radius, and the total drive force of the vehicle has to overcome the effects of all the resistance, and also the effects of gravity when the vehicle is traveling on a ramp. Assuming that the total driving force is equally distributed among the four tires, the required driving force for each tire is calculated as follows:

$$F > \frac{G \cdot f \cdot cos\alpha + G \cdot \mu \cdot cos\alpha + G \cdot sin\alpha}{4} \tag{7}$$

where:

F is the required driving force per tire, [N]; G is the weight of the whole vehicle, [mg]; f is the rolling resistance coefficient, which generally takes a value between 0.1 and 0.25; μ is the longitudinal maximum attachment coefficient for complete slip; α is the inclination angle of the ramp, [°].

Electrification conversion

Currently, the mainstream motor directions are permanent magnet synchronous motor and AC asynchronous motor. The seeder often repeatedly starts and stops, frequently accelerates and decelerates and the maximum running speed is small, so the permanent magnet synchronous motor is selected. The drive mode of the motor is shown in Fig. 6.

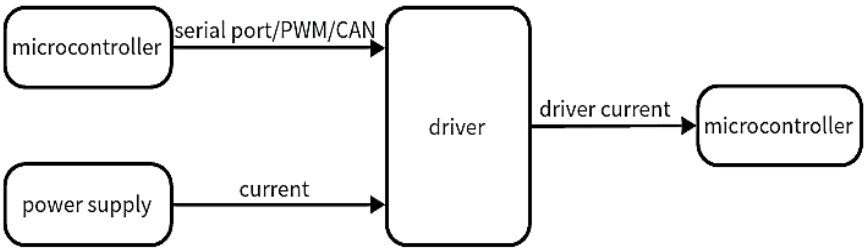

Fig. 6 - Motor drive type

Assuming that the traveling motor has no reducer, the rated speed of the drive motor is calculated as shown in Equation 8. The power required by the seeder when climbing a slope is greater than the power required for traveling in a straight line on level ground, so the rated power of the motor is based on the power required for climbing a slope as a reference, and the rated power is calculated based on Equation 7, as shown in Equation 9.

$$n = \frac{V_{max}}{2\pi r \times 0.8} \tag{8}$$

$$P = \frac{1}{0.96n}\left(\frac{f \cdot mg \cdot cos\,\alpha}{3600}V_{max} + \frac{mg \cdot sin\,\alpha}{3600}V_{max}\right) \tag{9}$$

where:

n is the number of motors; V_{max} is the maximum travel speed, [m/s]; r is the tire radius in Equation 8; P is the rated power of the motor, [W].

The minimum torque requirement for planter operation in a full-service environment is 80% of the rated torque requirement, and the minimum torque requirement necessary for operation on a ramp is the maximum, with the rated torque (T) calculated as follows:

$$T = mgr(f\cos\alpha + \sin\alpha)/(0.8n\eta) \quad (10)$$

The battery energy source of the planter is based on the original fuel tank capacity to select the ternary lithium battery with a weight of 160 kg and an energy density of about 200 Wh/kg, and the calculation of the battery's operating hours (H) under full charge is as follows:

$$H = 160 \times 200/(4P) \quad (11)$$

Overall design

The control system of the seeder is mainly designed, and the control system is divided into two parts: the motion control system and the main control system.

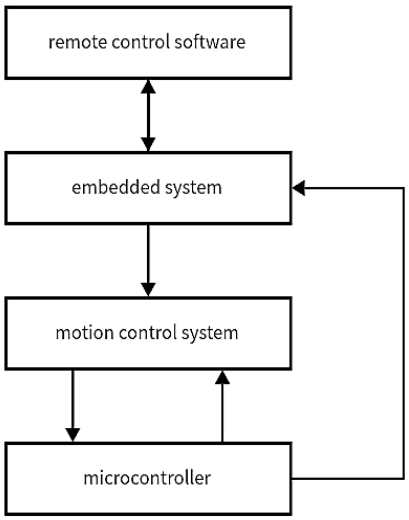

Fig. 7 - Structural sketch of the control system of the planter

Motion Control System

The motion control system is the core of the whole system, with a microcontroller as the main controller, choose the STM32F103 chip. The block diagram of the control system is shown in Figure 8. The microcontroller controls the motor rotation through the motor driver, and the communication method with the motor driver is selected as Pulse-width-modulation (PWM) control, and the PWM control method can reduce the system cost and power consumption *(Guo Yanhong, 2010)*. The resolution of the PWM control method is adjusted to 10 KHz in the simulation software. Speed monitoring of the actual speed of the motor is carried out through the Hall encoder, which uses a quadruple-frequency measurement method, which is not only highly resistant to interference but also capable of realizing accurate position control. The conversion relationship between the encoder value and the speed of the planter is calculated using the following method:

$$V = CONT \cdot \frac{1}{f} \cdot S \cdot \delta \quad (12)$$

where:

$CONT$ denotes the encoder count, f is the sampling rate, S is the tire circumference, and δ is the encoder accuracy.

From Equation 2 and Equation 3, it can be seen that the speed of the motor can be expressed by the linear speed and steering target angular speed. Therefore, the linear velocity and the steering target angular velocity are used as the control signals of the master control system and finally converted to the target signal of the motor. To compensate for the discontinuity of the sensor in time series data acquisition, the STM32 microcontroller discretizes the data by using the first order difference and iterative integral at the time of the timer interrupt, and the frequency at which the timer interrupt occurs in this study is set to 200 Hz. According to the discretized data, PID control can achieve the control of the motor. The motion control flowchart is shown in Figure 9.

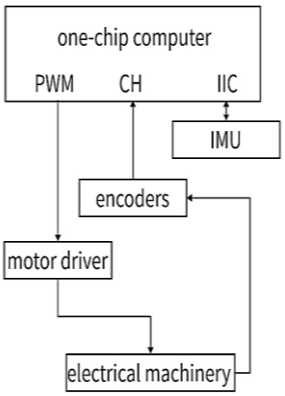

Fig. 8 - Motion control system diagram

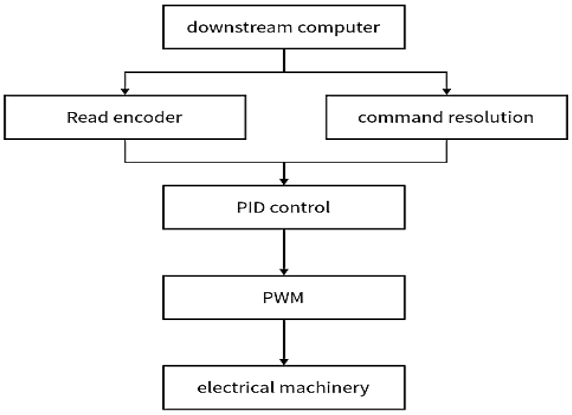

Fig. 9 - Motion control flowchart

The actual working conditions when the seeder is working are complex, to get the real condition of the vehicle, it is also necessary to use the MPU6050 module in the Inertial Measurement Module (IMU), which realizes the function of communicating with the microcontroller and connecting to other sensors through two IIC interfaces.

Master Control System

The main control system is developed using a high-performance embedded processor and an open-source operating system. The embedded system consists of a hardware layer, a driver layer, and a software layer. The hardware layer includes various hardware devices such as serial port, processor, camera, WIFI, etc.; the driver layer is responsible for providing the driver of the corresponding device in the hardware layer so that the upper layer of user software can call the hardware functions; the top layer is the user software layer, which is the place to realize the user's logical functions. In this layer, users can write code to realize various functions and logical operations.

The microcontroller communicates with the main control system through the serial port, mainly realizing the reception of control commands sent by the main control system and the sending of information collected by the sensors. This research considers the richness of the system ecology and the convenience of system editing and uses an embedded Linux system to complete the platform construction. Users can get the Linux source code for free, and then complete the transformation according to their own needs *(Lin Jimin, 2010)*. The WIFI driver is not included in the Linux source code and needs to be transplanted. The HI3881 WIFI chip is selected for WIFI, which has a standard broadband of 20 MHz and a maximum physical layer rate of 72.2 Mbit/s. The camera is equipped with the UVC protocol. The camera is equipped with UVC protocol devices, only in the source code for USB configuration and open the kernel module code. MJPG technology is selected for video monitoring, which is characterized by low performance requirements for the system and high clarity, and can simultaneously capture images and data output, which is suitable for field environments with complex working conditions.

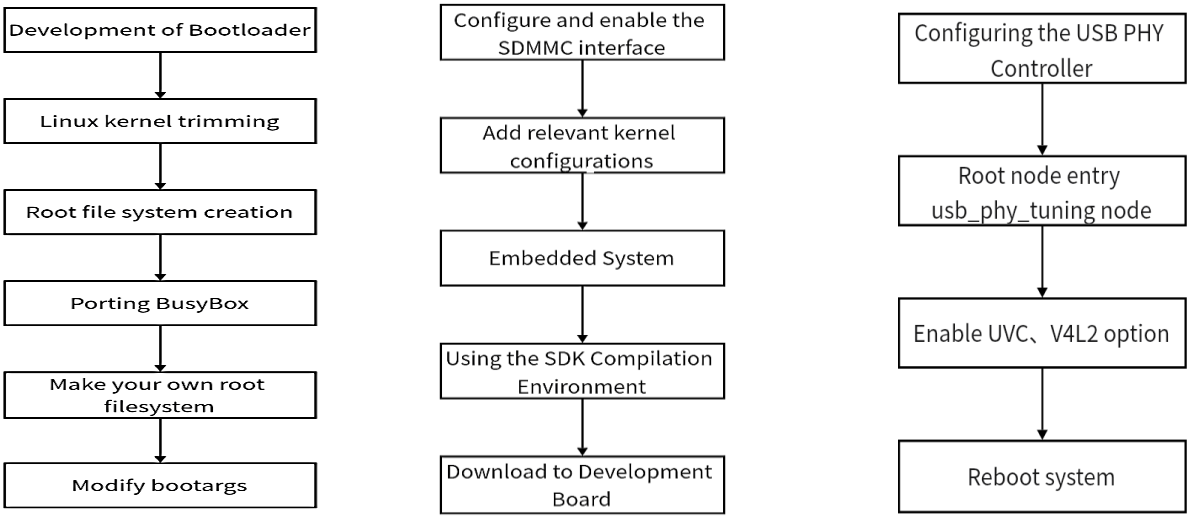

Fig. 10 - Embedded system, WIFI, and Camera operation steps

RESULTS

Control system stability test

This test selected the model vehicle for technical verification, the microcontroller as the core of the motion control system installed in the middle of the chassis mezzanine, and the main control system is installed in the ground above the front end of the vehicle placed in the camera used to monitor the road conditions. Based on the soil water content and soil density after irrigation and alkali reduction in Bayannur City provided by Inner Mongolia Dabo Jintian Machinery Co., Ltd, the test field was manually watered, and the test was conducted when the data from the soil temperature and humidity sensors were the same as the basic data.

Fig. 11 - Plow land

Fig. 12 - Flatten out the land

Fig. 13 - Comparison of land

Fig. 14 - Test model vehicles

Linear Offset Error Test

Straight-line offset error tests were conducted in a 40-meter-long test field, with 10 meters as a group for three sets of comparative tests. The starting point of the vehicle in each set of tests was 50 cm away from the edge of the test field, the edge of the test field was a straight line, and the attitude of the vehicle at the starting point was positioned parallel to the edge of the test field. In each group of experiments, a measurement point was set at every one-meter interval, and at each measurement point, the offset of the vehicle's straight driving was obtained by measuring the distance between the vehicle and the edge of the test field. The results of the experiments are shown in Fig. 15, which can be seen from the experimental results:

(1) With the increase of driving distance, the soil adhered to the tires of the model vehicle increases, resulting in a gradual increase in the amount of straight line offset, but due to the algorithm of bias correction, the offset error is within the design allowable error range of 10 cm.

(2) The vehicle is generally in a pothole each time the offset is large, and the increase in torque causes the vehicle to leave the pothole with a larger offset.

Table 1

Distance of rutting from the edge of the test field

Measuring point	The first time [cm]	The second time [cm]	The third time [cm]
0	50	50	50
1	50.4	50.8	50.5
2	49.9	51.5	50.3
3	49.6	51.2	50.0
4	49.8	50.7	50.4
5	49.4	51.1	50.5
6	49.0	51.4	49.9
7	48.6	50.9	49.0
8	48.9	49.3	49.4
9	48.2	49.7	49.9
10	48.7	49.3	49.3

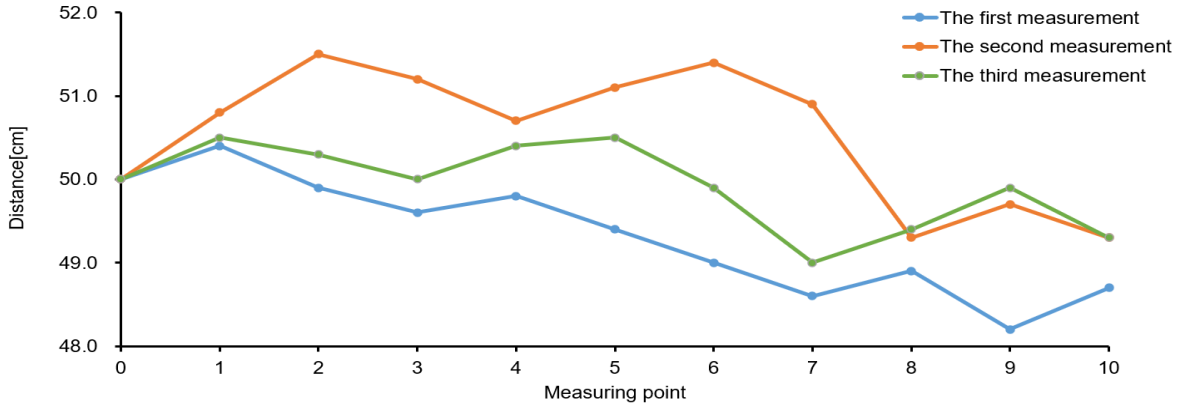

Fig. 15 - Plot of linear offsets for model vehicles

Fig. 16 - Trace diagrams for traveling in a straight line

Steering experiments on model vehicles

Tests were conducted on the model vehicle to evaluate its steering capabilities across different steering radii, including both large and small radii. The results suggest that the control system proposed in this study effectively facilitates the execution of steering maneuvers by the model vehicle, meeting diverse operational requirements with precision.

Fig. 17 - Trace diagrams for large-radius steering

Fig. 18 - Trace diagrams for small-radius steering

CONCLUSIONS

Aiming at the current problem of high dependence on manpower for seeders, the original diesel seeder was motorized from a practical point of view after dynamics and kinematics analysis. The control system of the planter was developed in two layers in the form of layered development. The control system is divided into the motion control system and the main control system, and the logic between the two systems is close and the division of labor is clear. The motion control system is based on the STM32 platform, which realizes the monitoring of the speed and motion attitude of the planter by cooperating with the encoder and IMU module; the master control system takes Linux as the platform, which realizes the communication with the motion control system and the monitoring of the working condition of the planter. The remote-control software realizes the function of human-machine interaction, which lays the foundation for the realization of unmanned driving. The stability test of the control system was carried out by using a model vehicle, and the test showed that the control system designed in this paper is stable and reliable, and meets the needs in actual production. Through the electrification of sunflower growing machinery and the design of the control system, the seeding machine can reduce the pollution of the environment and human injury.

ACKNOWLEDGEMENT

The authors were funded for this project by the Natural Science Foundation of Inner Mongolia Autonomous Region (No.2019MS03069).

REFERENCES

[1] Bi Yajuan, (2021). Comparison of advantages and disadvantages of rice machine direct seeding and machine transplanting and application considerations (水稻机直播与机插秧优缺点对比与应用注意事项). *Agricultural Machinery Use and Maintenance*, Vol. 11, pp. 155-156, China.

[2] Brenna M., Foiadelli F., Leone C., Longo M., and Zaninelli D., (2018). Feasibility proposal for heavy duty farm tractor. *2018 International Conference of Electrical and Electronic Technologies for Automotive*, pp. 1-6, Italy.

[3] Chen Huaxin, LI Shuai, (2024). Optimization of tractor hydraulic motor gears based on parametric design (基于参数化设计的拖拉机液压马达齿轮优化). *Agricultural Mechanization Research*, Vol. 46, pp. 233-237, China.

[4] Das A., Jain Y., Agrewale M.R.B., Bhateshvar Y.K., (2019). Design of a concept electric mini tractor. *2019 IEEE Transportation Electrification Conference*, pp. 1-7, India.

[5] Ding Dong, (2021). Research on slip steering control of small four-wheel independent drive vehicles (小型四轮独立驱动车辆滑移转向控制研究). *Xiamen Institute of Technology*. China.

[6] Guo Yanhong, (2010). Application of wireless sensor networks in building temperature monitoring system (无线传感器网络在楼宇温度监控系统中的应用研究). *Taiyuan University of Technology*, China.

[7] Gurusamy S.K. and Devaradjane G., (2015). Electrical tractive equipment design for small & marginal farm mechanization. *2015 IEEE International Transportation Electrification Conference (ITEC)*, pp. 1-6, India.

[8] Li Jun, Tang Shuang, Zhou Wei, (2019). A model predictive path tracking method considering vehicle stability (考虑车辆稳定性的模型预测路径跟踪方法). *Journal of Huaqiao University (Natural Science)*, Vol. 40, pp. 574-579, China.

[9] Liang Chao, Wang Hongzhen, Bao Xiaozhim, Zhang Qi. (2024). Research on a path tracking method for an autonomous seeder in paddy field (一种稻田自主播种机的路径跟踪方法的研究). *Agricultural Mechanization Research*, Vol. 46(03) pp. 52-56, China.

[10] Liang Lijun, et al. (2023). Development of 2BQD series of electrically-driven intelligent high-speed precision sowing machine (2BQD 系列电驱智能高速精播机的研制). *Agricultural Machinery Use and Maintenance*, Vol. 07, pp. 06-10, China.

[11] Lin Jimin, Wu Yi, Lin Xiao, (2010). Construction and application of Linux-based embedded system development platform (基于 Linux 嵌入式系统开发平台的构建及应用). *Modern Electronic Technology*, Vol.18, pp. 30-34, China.

[12] Lovarelli D. and Bacenetti J., (2019). Exhaust gases emissions from agricultural tractors: State of the art and future perspectives for machinery operators. *Biosystems Engineering*, Vol.186, pp. 204-213, Italy.

[13] Shen Peng, Cao Kai, Liu Bingzheng, et al, (2019). An unmanned path tracking method combined with a planning layer (一种结合规划层的无人驾驶路径跟踪方法). *Journal of Shandong University of Technology (Natural Science Edition)*, Vol. 33(06), pp. 50-55, China.

[14] Tahmish Fatima, Naveen Kumar Arora. (2021). Pseudomonas entomophila PE3 and its exopolys-accharides as biostimulants for enhancing growth, yield and tolerance responses of sunflower u-nder saline conditions. *Microbiological research*, Vol. 244, India.

[15] Xiong Yong, Zhang Jia, Huang Kaisheng, et al (2020). Optimal control-based path tracking method for dual-jet-propelled unmanned craft (基于最优控制的双喷推无人艇路径跟踪方法). *Ship Engineering*, Vol.42(02), pp. 20-27, China.

[16] Yang Yun, Liu Tingting (2022). Calculation of slip and path planning for agricultural robots based on machine learning (基于机器学习的农业机器人滑移量计算及路径规划). *Agricultural Mechanization Research*, Vol. 44(09), pp. 264-268, China.